


High-entropy grain boundaries

Jian Luo ¹✉ & Naixie Zhou¹

As high-entropy alloys receive an increasing amount of attention, an interesting scientific question arises: can grain boundaries be “high entropy”? In 2016, we proposed “high-entropy grain boundaries” as the grain boundary counterparts to high-entropy materials. Here, we discuss the underlying interfacial thermodynamics to elaborate relevant concepts. We emphasize that “high-entropy grain boundaries” are neither equivalent to grain boundaries in high-entropy materials nor simply “compositionally complex grain boundaries”, but they should possess specific thermodynamic characters. Using a simplified segregation model, we illustrate that both grain boundary and bulk high-entropy effects can reduce grain boundary energy with increasing temperature for saturated multicomponent alloys, where the effective grain boundary entropy can be positive and increase with the number of components. We show that high-entropy grain boundaries can stabilize nanocrystalline alloys at high temperatures via thermodynamic and kinetic effects. Grain boundary structural disordering and transitions may offer further opportunities to attain higher effective grain boundary entropies.

High-entropy alloys and ceramics (HEAs and HECs), which are subgroups of broader classes of compositionally complex (or complex concentrated) alloys and ceramics (CCAs and CCCs), have attracted substantial research interests recently^{1–7}. Here, we post an interesting scientific question: can an interface, particularly a grain boundary (GB), be “high entropy”? In 2016, we first proposed the concept and terminology of high-entropy grain boundaries (HEGBs) with a single numerical example in a Current Opinion article as a future perspective⁸. We subsequently showed that HEGBs can be utilized to stabilize nanocrystalline alloys (nanoalloys) at high temperatures⁹. While that original work⁹, particularly the idea of stabilizing nanoalloys with high-entropy effects, has caught substantial interests^{10–20}, a rigorous thermodynamic theory of HEGBs has not been presented. This article elaborates the relevant concepts and present a complete thermodynamic framework for the first time, and subsequently discusses the future perspective.

In a multicomponent system, a GB can certainly be compositionally complex. In fact, even if the bulk phase a conventional multicomponent alloy that is a dilute solid solution of multiple solute components, the GB can be a concentrated multi-principal component solution (Fig. 1c), thereby potentially being high entropy even if the bulk alloy is not. Here, we need to first discuss what is GB entropy and thermodynamic characters of HEGBs based on rigorous interfacial thermodynamics.

GB entropy and interfacial thermodynamics

There are two general ways to define GB entropy. In the classical Gibbs adsorption theory, we can define the GB excess of entropy (s^{xs}), which has a well-defined value (independent of the Gibbs dividing plane) for a GB. For a bulk phase of a closed system, entropy (S) measures how the Gibbs free energy (G) decreases with temperature (T) at a constant pressure (P): $S = -(\partial G/\partial T)_P$. Analogously, we look for a HEGB to have a positive and large “effective GB entropy”: $s_{GB}^{eff} \equiv -(\partial \gamma_{GB}/\partial T)_P$, where GB energy (γ_{GB}) decreases with increasing temperature.

¹Department of Nanoengineering; Program of Materials Science and Engineering, University of California San Diego, La Jolla, CA, USA. ✉email: jluc@alum.mit.edu

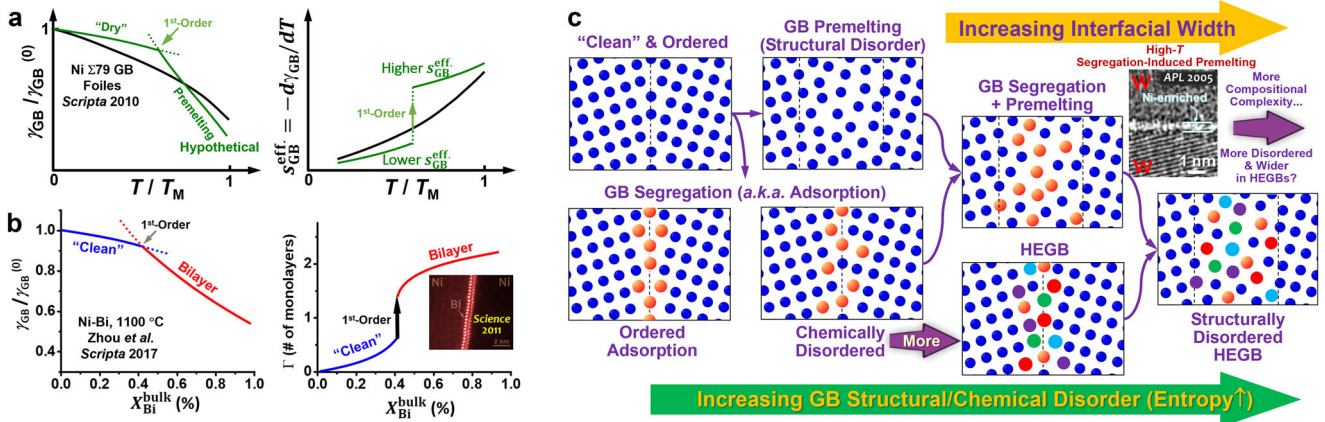


Fig. 1 Grain boundary (GB) disorder, adsorption, and entropy. **a** Normalized GB energy ($\gamma_{GB}/\gamma_{GB}^{(0)}$) and $d\gamma_{GB}/dT$ vs. normalized temperature (T/T_M) for a Ni Σ 79 GB (replotted after Foiles²¹ with permission ©Elsevier 2010) and a hypothetical case with a first-order GB premelting transition. **b** GB energy (γ_{GB}) and GB adsorption (Γ) vs. bulk Bi percentage (X_{Bi}^{bulk}) for a Bi-doped Ni general GB (replotted after Zhou et al.²³ with permission ©Elsevier 2017), where the inset is a scanning transmission electron microscopy image of Bi bilayer adsorption (reprinted after Luo et al.²⁹ with permission ©AAAS 2011). **c** Schematic illustration of different GB structures with increasing structural and/or chemical disorder and entropy. Insets are high-resolution transmission electron microscopy images showing coupled GB premelting and segregation in Ni-doped W (reprinted after Luo et al.³⁰ with permission ©AIP 2005).

This also represents a beneficial feature to stabilize nanoalloys at high temperatures. However, a multicomponent GB is more complex (than a bulk phase) because it is not a closed system. Different scenarios will be discussed subsequently.

In an N -component system, interfacial energy (γ) is the interfacial excess of grand potential:

$$\gamma = u^{xs} - T s^{xs} - \sum_{i=1}^N \mu_i \Gamma_i, \quad (1)$$

where u^{xs} , s^{xs} , and Γ_i are the interfacial excess of internal energy, entropy, and (adsorption of) the i -th component ($i = 1, 2, \dots, N$), respectively, based on the Gibbs definition. For a phase boundary, we can select the Gibbs dividing plane so that $\Gamma_1 = 0$. However, this convention cannot be adopted for a GB, where two abutting grains are the same phase, so that the GB excess quantities are independent of the position of the Gibbs dividing plane. The generalized Gibbs adsorption equation states:

$$d\gamma_{GB} = -s^{xs} dT + \bar{V} dP - \sum_{i=1}^N \Gamma_i d\mu_i. \quad (2)$$

For a specific GB in a unary system, its GB energy varies with temperature at a constant pressure:

$$\left(\frac{\partial \gamma_{GB}}{\partial T}\right)_P = -s^{xs} - \Gamma \left(\frac{d\mu}{dT}\right)_P = -(s^{xs} - \Gamma \bar{S}), \quad (3)$$

where \bar{S} is molar entropy. Since $\Delta v_{GBfree} = -\Gamma \bar{V} = (\partial \gamma_{GB} / \partial P)_T$ is the GB “free volume” per unit area (in a unit of length), we may define the effective GB entropy for a unary GB as:

$$s_{GB}^{eff} \equiv -\left(\frac{\partial \gamma_{GB}}{\partial T}\right)_P = s^{xs} + (\bar{S} / \bar{V}) \cdot \Delta v_{GBfree} = s^{xs} + S_V \cdot \Delta v_{GBfree}, \quad (4)$$

where $S_V = (\bar{S} / \bar{V})$ is the volumetric entropy of the bulk phase. It is interesting to note that $s_{GB}^{eff} \equiv -(\partial \gamma_{GB} / \partial T)_P \neq s^{xs}$ even for a simple unary GB (because $\Gamma \neq 0$). This inequality is a unique character of unary GBs since we would typically select the Gibbs dividing plane to ensure $\Gamma = 0$ for other types of unary interfaces (e.g., unary solid-liquid and solid-vapor interfaces), so that $s_{GB}^{eff} = s^{xs}$ for those cases. For an unary GB, s_{GB}^{eff} is typically positive because the GB region is usually more disordered ($s^{xs} > 0$) and less dense ($\Gamma < 0$ and $\Delta v_{GBfree} > 0$) than the

crystal. This suggests that GB energy generally decreases with increasing temperature or $(\partial \gamma_{GB} / \partial T)_P < 0$ for a unary GB, as evident by the atomistic simulation of a Ni GB by Foiles (Fig. 1a)²¹. If a first-order GB premelting transition occurs, a “liquid-like” GB complexion²² (a.k.a. 2D interfacial phase) with a high s_{GB}^{eff} can form (Fig. 1a).

For a multicomponent system, the Gibbs-Duhem equation states:

$$\sum_{i=1}^N X_i^{bulk} d\mu_i = -\bar{S} dT + \bar{V} dP, \quad (5)$$

Combining Eqs. (2) and (5) at a constant pressure ($dP = 0$) produces:

$$d\gamma_{GB} = -\left[s^{xs} - \left(\frac{\Gamma_1}{X_1^{bulk}}\right) \bar{S}\right] dT - \sum_{i=2}^N \left[\Gamma_i - \left(\frac{X_i^{bulk}}{X_1^{bulk}}\right) \Gamma_1\right] d\mu_i. \quad (6)$$

Here, we note that for multicomponent systems, chemical potentials (μ_i 's) depend on both temperature and the bulk composition (X_i^{bulk}). For an ideal solution, we can obtain:

$$\begin{aligned} \left(\frac{\partial \gamma_{GB}}{\partial X_i^{bulk}}\right)_{P,T,X_j(j \neq 1; j \neq i)} &= -\frac{RT}{X_i^{bulk}} \left[\Gamma_i - \left(\frac{X_j^{bulk}}{X_1^{bulk}}\right) \Gamma_1\right] \\ &= -RT \left[\frac{\Gamma_i}{X_i^{bulk}} - \frac{\Gamma_1}{X_1^{bulk}}\right]. \end{aligned} \quad (7)$$

where R is gas constant. Taking Component 1 as the principal element (in a conventional multicomponent alloy), Eq. (7) suggests that increasing amount of segregation ($\Gamma_i > 0$, while $\Gamma_1 < 0$) can reduce GB energy γ_{GB} . This is illustrated by a binary example of Bi-doped Ni in Fig. 1b, which further shows the occurrence of a first-order GB adsorption transition that accelerates the GB energy reduction with increasing doping²³.

Let us consider the temperature dependence of GB energy, where we can treat two limiting cases. First, for a fixed bulk composition (i.e., below the solvus or solubility limit for all

components), applying the chain rule to Eq. (2) produces:

$$\left(\frac{\partial \gamma_{GB}}{\partial T}\right)_{P, \mathbf{X}^{\text{bulk}} (X_j^{\text{bulk}} \text{ } j=1,2,\dots,N)} = -s^{\text{xs}} - \sum_{i=1}^N \Gamma_i \left(\frac{\partial \mu_i}{\partial T}\right)_{P, \mathbf{X}^{\text{bulk}}} \quad (8)$$

$$= -\left(s^{\text{xs}} - \sum_{i=1}^N \Gamma_i \bar{S}_i\right),$$

where \bar{S}_i is the partial molar entropy of the i -th component, and \mathbf{X}^{bulk} is bolded to represent the bulk composition vector of a multicomponent alloy). For a strong segregating system, GB energy often increases with increasing temperature because of temperature-induced desorption that reduces γ_{GB} (at least in the lattice model presented here without considering GB structural disordering, the effects of which can potentially reverse this trend and will be discussed later), thereby resulting in a negative effective $s_{GB}^{\text{eff. (fixed } \mathbf{X}^{\text{bulk}})}$ (while s^{xs} can still be positive).

Second, we may consider a case of a saturated conventional multicomponent alloy with one principal and $(N - 1)$ segregating solute components. Here, with changing temperature, the composition of the grains moves along the maximum solvus line, where the chemical potentials of all solutes are pinned by a set of $(N - 1)$ precipitates (assumed, for simplicity, to be stoichiometric line compounds). If chemical potentials μ_j ($j \neq 1$) are fixed (as an

approximation), we can derive from Eq. (6):

$$\left(\frac{\partial \gamma_{GB}}{\partial T}\right)_{P, X_j(T) \text{ on solvus}} \approx \left(\frac{\partial \gamma_{GB}}{\partial T}\right)_{P, \mu_j (j \neq 1)} \quad (9)$$

$$= -\left[s^{\text{xs}} - \left(\frac{\Gamma_1}{X_1^{\text{bulk}}}\right) \bar{S}\right] \equiv -s_{GB}^{\text{eff. (saturated)}}.$$

For a segregating system, $s_{GB}^{\text{eff. (saturated)}}$ is likely positive since we typically expect: $s^{\text{xs}} > 0$ and $\Gamma_1 < 0$.

GB high-entropy effects in a simplified segregation model

To illustrate GB and bulk high-entropy effects, we can use a statistical thermodynamic model for multicomponent GB segregation (*a.k.a.* adsorption)⁸ that is a generalization of the binary Wynblatt-Chatain model²⁴ with a few simplifications. Considering a general twist GB with segregation limited to the two layers at the GB core and further assuming an ideal solution for simplicity (that can be further refined to include multilayer adsorption and regular-solution interactions⁸), we can obtain:

$$\left\{ \begin{array}{l} \gamma_{GB} = \gamma_{GB}^{(0)} + 2n_{PD} \sum_{i=2}^N X_i^{GB} \Delta g_i^{\text{seg.}} + 2n_{PD} \sum_{i=1}^N kT X_i^{GB} \ln \left(\frac{X_i^{GB}}{X_i^{\text{bulk}}}\right) \\ \frac{X_i^{GB}}{X_i^{\text{bulk}}} = \frac{X_i^{GB}}{X_i^{\text{bulk}}} \exp \left(-\frac{\Delta g_i^{\text{seg.}}}{kT}\right) \end{array} \right. \quad (10)$$

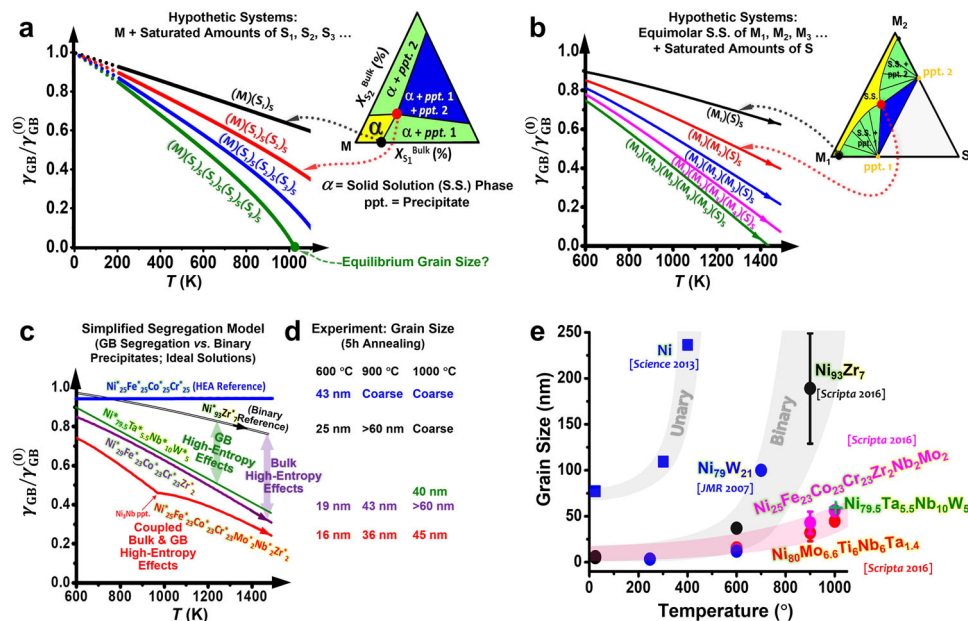


Fig. 2 Grain boundary (GB) and bulk high-entropy effects in high-entropy grain boundaries (HEGBs). **a** Computed normalized GB energy ($\gamma_{GB}/\gamma_{GB}^{(0)}$) vs. temperature (T) curves showing that a GB high-entropy effect can decrease $d\gamma_{GB}/dT$ along the solvus line in a hypothetical conventional multicomponent nanoalloy with one principal (M) and multiple segregating (S_i) elements. This GB high-entropy effect increases with increasing number of segregating elements. **b** Computed $\gamma_{GB}/\gamma_{GB}^{(0)}$ vs. T curves along the bulk solvus curves, showing that γ_{GB} can also be reduced via a bulk high-entropy effect that lower the bulk chemical potentials to suppress precipitation to promote GB adsorption for a hypothetical high-entropy nanoalloy of 1–5 principal (M_i) and one segregating element (S). In **(a and b)**, subscript “S” indicates the bulk composition of the segregating element is kept saturated (on the solvus line) at each temperature. **c** Computed $\gamma_{GB}/\gamma_{GB}^{(0)}$ vs. T curves for several “Ni-like” alloys, where the superscripts “*” are used to note that the calculations were conducted by using a lattice model of ideal solutions with segregation enthalpies and bonding energies mimic the real alloys to capture useful trends. **d** Selected experimental results of measured grain sizes of nanoalloys annealed at three different temperatures for 5 h, which shows a correlation between reduced GB energies and grain sizes. **e** Experimentally measured grain size vs. annealing temperature curves for several nanoalloys with HEGBs along with Ni and Ni-based binary nanoalloys for comparison⁹. The numerical and experimental results are replotted or regenerated using the same procedures; the figure panels are reprinted or replotted after Zhou et al.^{8, 9}, both with permission ©Elsevier 2016.

where $\gamma_{GB}^{(0)}$ is the GB energy of the pure Component 1, n_{PD} is the planar density of atoms, and $\Delta g_{i \rightarrow 1}^{seg.}$ is the free energy change of GB segregation by swapping an atom of the i -th element inside the grain with an atom of the 1st element at the GB. Here, we adopt the sign convention that $\Delta g_{i \rightarrow 1}^{seg.} = \Delta h_{i \rightarrow 1}^{seg.} - T\Delta s_{i \rightarrow 1}^{seg.} \approx \Delta h_{i \rightarrow 1}^{seg.} < 0$ for positive GB segregation (while noting that positive $\Delta h_{i \rightarrow 1}^{seg.}$ values are sometimes cited in literature for GB enrichment). While we recognize the importance of GB segregation entropy $\Delta s_{i \rightarrow 1}^{seg.}$ ^{25–27}, it produces a temperature-independent segregation term (Eq. (10)) that affect $\partial\gamma_{GB}/\partial T$ only indirectly. Thus, we focus on $\Delta h_{i \rightarrow 1}^{seg.}$ (that is normally the larger and dominating term in $\Delta g_{i \rightarrow 1}^{seg.}$) here and will discuss $\Delta s_{i \rightarrow 1}^{seg.}$ (that were elaborated by Lejček et al.^{25–27}) latter. We also note that this model does not consider interfacial structural disorder so that $\gamma_{GB}^{(0)}$ is independent of temperature (albeit it should exhibit a negative temperature dependence due to interfacial disordering and GB free volume, as shown in Fig. 1a and Eq. (3)). Equation (10) suggests no “high-entropy effect” for $s_{GB}^{eff. (fixed X^{bulk})}$ (that is likely negative due to temperature-induced desorption) in this model without considering GB disordering: e.g., in a simple analysis assuming $(N - 1)$ segregating solutes of a fixed total amount of solutes $\sum_{i=2}^N X_i^{bulk}$ and identical $\Delta h_{i \rightarrow 1}^{seg.}$ (and therefore X_i^{GB}/X_i^{bulk}), both γ_{GB} and $s_{GB}^{eff. (fixed X^{bulk})}$ are independent of N . However, $s_{GB}^{eff. (saturated)}$ can be positive and increase with increasing N .

To analytically illustrate a GB high-entropy effect in a dilute multicomponent alloy, we can analyze a hypothetical ideal solution with one principal (M) and $(N - 1)$ segregating solute (S_i) elements (i.e., the bulk phase is not a HEA, referred to as “Type I” here). For a saturated N -component alloy in an equilibrium with $(N - 1)$ precipitates (i.e., the bulk composition moves along the maximum solvus line following $X_{i,solvus}^{bulk} \approx \exp(\Delta g_i^{sol./ppt.}/kT)$ for $i = 2, 3, \dots, N$, where $\Delta g_i^{sol./ppt.} < 0$ is the free energy of dissolving i from the precipitate), we can derive an approximated expression at the dilute limit ($\sum_{i=2}^N X_i^{bulk} \ll 1$) as:

$$\begin{cases} \frac{X_1^{GB}}{X_1^{bulk}} \approx \exp\left(-\frac{\Delta g_1^{seg.-ppt.}}{kT}\right) \\ \gamma_{GB} - \gamma_{GB}^{(0)} \approx 2n_{PD}kT \ln X_1^{GB} \approx -2n_{PD}kT \ln\left[1 + \sum_{i=2}^N \exp\left(-\frac{\Delta g_i^{seg.-ppt.}}{kT}\right)\right] \end{cases} \quad (11)$$

where $\Delta g_i^{seg.-ppt.} (= \Delta g_{i \rightarrow 1}^{seg.} - \Delta g_i^{sol./ppt.})$ represents the free energy difference between the segregation and precipitation per atom. Here, an empirical relationship (for the enthalpic part) exists: $\Delta g_i^{seg.-ppt.} \approx -(0.10 \pm 0.06)$ eV/atom (or $-(10 \pm 6)$ kJ/mol)²⁸. Equation (11) suggests that adding more segregating elements can reduce γ_{GB} along the solvus line for a N -component system (i.e., increase the effective GB entropy $s_{GB}^{eff. (saturated)}$), representing a GB high-entropy effect.

Furthermore, we can conduct numerical experiments to show this GB high-entropy effect using typical parameters for transition metals (using similar parameters as the case shown in Fig. 6 in Ref. 8, but for a simpler ideal solution in an equilibrium with $(N - 1)$ precipitates of 1:1 stoichiometric $(M)_1(S_i)_1$ of identical (significant) $\Delta g_i^{sol./ppt.}$ of -0.13 eV/atom and an intermediate $\Delta g_{i \rightarrow 1}^{seg.}$ similar to those for Nb or Ta in Ni). Figure 2a shows this GB high-entropy effect of enhanced reduction in γ_{GB} with more segregating elements. Similar results were obtained in a regular-solution model previously⁸.

Bulk high-entropy effects and type II HEGBs

In addition, we can show a bulk high-entropy effect for HEAs with multiple principal elements (i.e., the grains are HEAs) and at

least one (or more) segregating elements to form “Type II” HEGBs (Fig. 2b)⁹. Prior numerical experiments (Fig. 2b)⁹ of a hypothetical symmetric ideal solution with $(N - 1)$ principal (M_i , assumed to have identical properties for simplicity) and one (S) segregating elements based on the same model described above illustrate that γ_{GB} can also be reduced via a bulk high-entropy effect. This bulk high-entropy effect lowers the bulk chemical potentials to suppress precipitation to promote more GB adsorption for the HEAs saturated with the segregating element S . Moreover, increasing the number of principal elements in HEAs enhances this bulk high-entropy effect to attain more negative ($\partial\gamma_{GB}/\partial T$)_{saturated}, as shown in Fig. 2b. Similar to the prior case, we can also derive an approximated analytical expression for an ideal solution at the dilute limit ($X_N^{bulk} \ll 1$; $X_i^{bulk} = (1 - X_N^{bulk})/(N - 1) \approx 1/(N - 1)$ for $i = 1, 2, \dots, (N - 1)$) for a Type II HEGB in a HEA:

$$\gamma_{GB} - \gamma_{GB}^{(0)} \approx 2n_{PD}kT \ln\left(\frac{X_1^{GB}}{X_1^{bulk}}\right) \approx -2n_{PD}kT \ln\left[1 + (N - 1)^{x/y} \exp\left(-\frac{\Delta g_N^{seg.-ppt.}}{kT}\right)\right] \quad (12)$$

Here we assume, for simplicity, all binary i - N systems ($i = 1, 2, \dots, (N - 1)$) have identical thermodynamic parameters and the binary solvus lines are pinned by stoichiometric $(M_i)_x(S)_y$ precipitates following $X_{i,binary solvus}^{bulk} \approx \exp(\Delta g_N^{sol./ppt.}/kT)$, so that the bulk solubility limit of the segregating N -th component is given by: $X_N^{bulk} = (N - 1)^{x/y} \exp(\Delta g_N^{sol./ppt.}/kT)$. Equation (12) suggests that more principal elements can also reduce γ_{GB} along the solvus line (i.e., increase the effective GB entropy $s_{GB}^{eff. (saturated)}$). This represents a bulk high-entropy effect for Type II HEGBs with HEA grains.

We should note that this bulk high-entropy effect and Type II HEGBs may also exist in conventional HEAs if one (or more) of the principal element(s) segregates at GBs. An assessment by Miracle and Senkov³ suggested that slow bulk diffusion in HEAs may not supported by the available data; in fact, the term “sluggish kinetics” was initially introduced based on the observations of fine grains in HEAs. Here, we hypothesize that the “sluggish” grain growth kinetics can exist HEAs because of this bulk high-entropy effect (with the formation of Type II HEGBs), which should be further examined in future studies.

Interfacial structural disordering and GB transitions

The segregation model discussed above do not consider GB structural disordering, which can further increase GB entropy. In addition, first-order GB transitions (e.g., a first-order GB segregation transition for Ni-Bi²⁹ shown Fig. 1b and a hypothetical first-order GB premelting transition shown in Fig. 1a) can take place to accelerate the reduction in γ_{GB} . GB structural disordering and segregation can be coupled, as observed in W-Ni (Fig. 1c)³⁰. It is yet unknown when (and why) ordered (Ni-Bi)²⁹ vs. disordered (W-Ni)³⁰ segregation structures form at GBs. We anticipate that structurally disordered HEGBs can possess even higher effective GB entropies with increased interfacial width (Fig. 1c) and potentially exhibit positive $s_{GB}^{eff. (fixed X^{bulk})}$ (that is negative at a fixed grain composition in the lattice model discussed above that does not consider GB disordering effect) to show GB high-entropy effects. This is an area that is largely unexplored and will be discussed further in the Outlook section.

Definitions and terminologies

Similar to bulk HEAs, the definition of HEGBs can be debatable. Here, we propose to first define “compositionally complex GBs (CCGBs)” as GBs with at least five principal components (e.g., >5%) at the GB core, as the GB counterpart to the bulk CCAs or CCCs. Then, we may loosely define HEGBs as the GBs with large,

positive effective GB entropy ($s_{GB}^{eff} \equiv -\partial\gamma_{GB}/\partial T$). It is important to note that effective s_{GB}^{eff} can be either positive and negative in multicomponent alloys (vs. bulk configurational entropy that is always positive), and it also depends on the bulk phase equilibrium condition (e.g., fixed grain composition vs. saturated with secondary precipitation phases: $s_{GB}^{eff}(\text{fixed } X^{bulk}) \neq s_{GB}^{eff}(\text{saturated})$). At this time, we are reluctant to suggest a specific cut-off value in s_{GB}^{eff} to define HEGBs (that would be highly subjective). Instead, we propose two essential characters that help to define HEGBs: (1) the effective $s_{GB}^{eff} \equiv -\partial\gamma_{GB}/\partial T$ of HEGBs should be positive and (2) it should increase with increasing number of (segregating and/or primary) components, which can be achieved via the GB and/or bulk high-entropy effects discussed above.

Unlike the bulk phases, more principal components at the GB core (in CCGBs) do not always lead to larger (or even positive) $s_{GB}^{eff} \equiv -\partial\gamma_{GB}/\partial T$ for GBs. The configurational entropy at the GB core and the effective GB entropy (s_{GB}^{eff}) are not always positively correlated. In fact, CCGBs (in both HEAs and conventional multicomponent alloys) can have negative s_{GB}^{eff} so that they cannot be considered as HEGBs even if there are five or more components of nearly equimolar fractions at the GB core.

These unique characters (somewhat differing from bulk CCAs vs. HEAs) make the thermodynamics of CCGBs and HEGBs intriguing and interesting, calling for further theoretical, modeling, and experimental studies.

Stabilizing nanoalloys at high-temperatures via HEGBs

While HEGBs may have several unique characters, one potential application is to utilize them to stabilize nanoalloys at high temperatures⁹. To test this, we modeled, and subsequently fabricated and tested, several Type I (e.g., $Ni_{79.5}Ta_{5.5}Nb_{10}W_5$) and Type II (e.g., $Ni_{29}Fe_{23}Co_{23}Cr_{23}Zr_2$) multicomponent nanoalloys to show substantially improved high-temperature stability (Fig. 2c–e)⁹.

Here, we can simulate multicomponent alloys via adopting (1) the above simplified GB segregation model, (2) estimated GB and bonding energies as well as $\Delta s_{i \rightarrow 1}^{seg.}$ for the actual alloys, and (3) binary solvus lines based on empirical $\Delta g_i^{seg.-ppt.}$ or experimental phase diagrams to forecast useful trends⁹. Here, we use subscript “*” (e.g., “ $Ni_{25}Fe_{23}Co_{23}Cr_{23}Mo_{2}Nb_{2}Zr_{2}$ ”) to denote that they are ideal solutions that mimic the real alloys. Figure 2c suggests both GB and bulk high-entropy effects in reducing γ_{GB} , in comparison with benchmarks, for several alloys⁹. Subsequent experiments found that both Type I and Type II nanoalloys with HEGBs exhibit improved (sometime superior) high-temperature stabilities⁹. For example, $Ni_{25}Fe_{23}Co_{23}Cr_{23}Mo_2Nb_2Zr_2$ (with four principal and three segregating elements) maintained ~45 nm grain size after 5 h annealing at 1000 °C, outperforming not only their binary counterparts ($Ni_{79}Zr_{21}$ and $Ni_{93}Zr_7$) but also the conventional HEA counterpart ($Ni_{25}Fe_{25}Co_{25}Cr_{25}$), as shown in Fig. 2d, e⁹. This modeling and experimental validation methodology can be extended to other alloys in future studies.

We should note that there are two general approaches to inhibit grain growth: (1) thermodynamic stabilization by reducing γ_{GB} via solute segregation can reduce the grain growth driving force and (2) kinetic stabilization by solute drag and/or Zener (particle) pinning^{31, 32}. Notably, in the cases shown in Fig. 2c, GB energies, although being reduced by the HEGBs, are still significant (non-zero). Thus, kinetic stabilization should exist and be important.

A $Ni_{80}Mo_{6.6}Ti_6Nb_6Ta_{1.4}$ alloy was designed to further examine kinetic effects, where the Ti, Nb and Ta contents were about 60–70% of the binary solvus at 900 °C while Mo was ~25% of binary solid solubility⁹. Thus, this case resembles the fixed bulk composition scenario represented by Eq. (8) with no or little anticipated GB high-entropy effect (or the GBs in $Ni_{80}Mo_{6.6}Ti_6Nb_6Ta_{1.4}$ are CCGBs but not HEGBs). However, a prior

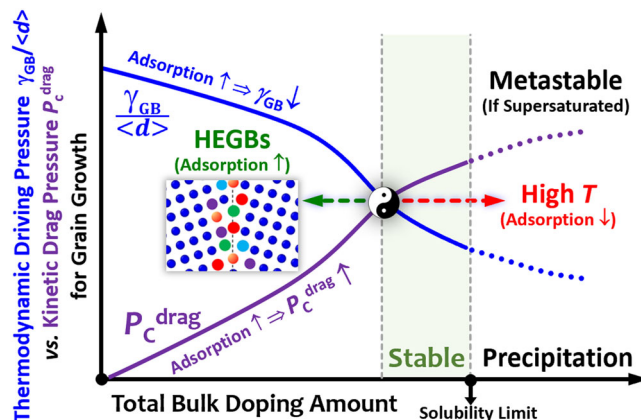


Fig. 3 Stabilizing nanoalloys at high temperatures with high-entropy grain boundaries (HEGBs). Schematic illustration of a balance of reduced thermodynamic driving pressure ($\gamma_{GB}/\langle d \rangle$, where γ_{GB} is grain boundary energy and $\langle d \rangle$ is the mean grain size) and increased critical kinetic solute drag pressure (P_C^{drag}) for grain growth, which result in the stabilization of a nanoalloy against grain growth. This balance has to be achieved before precipitation (below the solubility limit if the nanoalloy is at a thermodynamic equilibrium). Increasing temperature (T) can induce GB desorption (de-segregation) that moves the balance point toward right (to de-stabilize the nanoalloy, albeit the solubility limits also increase with increasing temperature). The HEGB-stabilized grain boundary segregation can counter the thermally induced desorption. The increased total adsorption (the total amount of all segregating components) at HEGBs, which can be more stable at high temperatures with increasing number of components, can simultaneously reduce the thermodynamic driving force and increase the kinetic solute drag, thereby increasing the high-temperature stability (or moving the balance point toward left). Interfacial disordering (illustrated in Fig. 1c) can further alter the thermodynamic and kinetic stabilities of nanoalloys at high temperatures.

experiment showed that this nanoalloy possessed a superior high-temperature stability, maintaining 45 nm grain size after annealing 1000 °C for 5 h (Fig. 3d, e)⁹. Here, the kinetic effects, particularly solute drag^{33, 34} (since binary phase diagrams suggest no precipitate above ~700 °C), presumably played the key role in stabilizing this nanoalloy.

Figure 3 shows that a stable nanoalloy can be achieved via a balance between the thermodynamic driving pressure ($\gamma_{GB}/\langle d \rangle$, where $\langle d \rangle$ is the mean grain size) and critical kinetic solute-drag pressure (P_C^{drag} , i.e., the maximum drag force solutes can impose on the GB before it tears itself off in the Cahn–Lücke–Stüwe model^{33, 34}): $\gamma_{GB}/\langle d \rangle = P_C^{drag}$. However, both the thermodynamic stabilization and kinetic solute drag become less effective at high temperatures due to temperature-induced GB desorption, which moves the balance point in Fig. 3 toward right. Here, HEGBs may boost GB adsorption to counter the thermally induced desorption (to move the balance point in Fig. 3 toward left to allow a larger stable window). Specifically, HEGBs can accommodate a higher total amount of GB adsorption within the bulk solid solubility limit (enhanced at high temperatures with more components, as shown in Fig. 2a, b). This effect can not only reduce the thermodynamic driving force for grain growth by decreasing γ_{GB} at high temperatures, but also enlarge solute drags to pin grain growth kinetically in “sluggish” HEGBs. We recognize that Zener (particle) pinning is another kinetic stabilization effect (not yet considered in Fig. 3).

Outlook

The theory of HEGBs is still in its infancy stage. Although the concept of HEGBs was proposed in 2016 with some modeling

and experimental supports^{8, 9}, which has caught substantial interests since then^{10–20, 25, 35, 36}, this current article is the first comprehensive discussion of the underlying thermodynamic theory (yet with simplified models). Thermodynamic and kinetic models of HEGBs should be developed and improved to guide this exploration and enable rigorous data analysis.

The multicomponent segregation model presented here, although they can illustrate important concepts and predict some useful trends, is highly simplified. Here, several improvements should be made in future studies. First, multilayer segregation and regular-solution interactions can be readily included, but analysis of a multicomponent system posts a challenge. For a N -component system, there are $N \times (N - 1)/2$ regular-solution (pair-interaction) parameters, e.g., there will be 10 pair-interaction parameters for a 5-component system! This will lead to complex (yet interesting) phenomena that should simulate future studies. Second, such pair interactions can result in ordering and clustering at GBs (as shown, e.g., in a recent study of GBs in HEAs³⁷), which can reduce the configurational entropy at GBs. Third, GB segregation entropy ($\Delta s_{i \rightarrow 1}^{\text{seg}}$)^{25–27} should also be considered to better model GB segregation. Here, we note that GB segregation entropy ($\Delta s_{i \rightarrow 1}^{\text{seg}}$) and the effective GB entropy ($s_{\text{GB}}^{\text{eff}} \equiv -\partial \gamma_{\text{GB}}/\partial T$) are two important GB-related entropies with different meanings. This Perspective article discusses the latter ($s_{\text{GB}}^{\text{eff}}$), but we recognize that GB segregation entropy ($\Delta s_{i \rightarrow 1}^{\text{seg}}$) can play an important role in determining GB segregation behaviors (thereby affecting $\partial \gamma_{\text{GB}}/\partial T = -s_{\text{GB}}^{\text{eff}}$, albeit somewhat indirectly as it produces a temperature-independent segregation according to Langmuir-MacLean type Eq. (10)). Interested readers are referred to Prof. Lejček et al.' articles^{25–27} for in-depth discussion of GB segregation entropy ($\Delta s_{i \rightarrow 1}^{\text{seg}}$).

Moreover, GB structural disordering, which is not considered in this segregation model, offers a further opportunity to attain even higher effective GB entropies. For example, while the lattice segregation model without considering interfacial disordering suggests no GB high-entropy effect for the fixed grain composition scenario ($s_{\text{GB}}^{\text{eff. (fixed } X^{\text{bulk}})} < 0$), coupled interfacial disordering and segregation of multiple species, which can enhance each other, may alter the high-temperature behaviors to allow decreasing γ_{GB} (and increasing total adsorption amount) with increasing temperature even with a fixed grain composition (to allow $s_{\text{GB}}^{\text{eff. (fixed } X^{\text{bulk}})} > 0$). This possibility (hypothesis) is yet to be tested by modeling and experiments. A more rigorous model of HEGBs should consider both chemical and structural (disordering) effects. Developing models for HEGBs in ceramics, which are more prone to form amorphous-like (structurally disordered) GBs³⁸, represents another challenge and opportunity.

Here, a future opportunity is to utilize GB disordering and transitions to tailor HEGBs and subsequently the high-temperature stability of nanoalloys (and other properties). Notably, Rupert's group showed the formation of amorphous-like GBs in W-doped Ni³⁹, Cu-Zr-Hf⁴⁰, and most recently in Cu-Zr-Hf-Nb-Ti and similar quinary nanoalloys²⁰ that enhance their high-temperature stability. This suggests a possibility to form structurally disordered (amorphous-like) HEGBs with even higher GB entropies to further enable exceptional high-temperature nanoalloy stability and other exotic properties (e.g., improved mechanical properties with amorphous-like GBs^{41, 42}). Amorphous-like intergranular films, first discovered in W-Ni (Fig. 1c) and Mo-Ni for metals (as segregation-induced GB premelting or prewetting)^{30, 43}, which are more commonly observed in ceramics³⁸, can enable (accommodate) more adsorption. A series of other GB complexions (*a.k.a.* 2D interfacial phases)^{22, 29, 44–47} may also exist in HEGBs, leading to different properties and opportunities.

A recent report showed the feasibility of combining atomistic simulations and machine learning to predict GB segregation and GB disorder for HEAs in a 5D space (as functions of temperature and four independent compositional degrees of freedom for quinary alloys), where a key observation is the coupling of GB segregation and disordering (that may further increase the effective GB entropy as discussed about)⁴⁸. Such methods can be used to model HEGBs more realistically and accurately than simplified models. Notably, GB “phase” diagrams have been computed for binary, multicomponent, and high-entropy alloys, representing a potentially transformative research direction⁴⁹. We envision that such GB diagrams may also be constructed to represent the temperature- and composition-dependent formation of both classes of HEGBs, as well as their thermodynamic, structural, and other properties in future studies.

Notably, Weismuller proposed the existence of an “equilibrium” grain size when the effective γ_{GB} approaches zero;⁵⁰ yet, Kirchheim⁵¹ suggested (based on the empirical relationship $\Delta G_i^{\text{seg.} - \text{ppt.}} \approx -(10 \pm 6) \text{ kJ/mol}$ ²⁸ that the equilibrium grain sizes in binary alloys often represent metastable states in supersaturated regions if and only if the precipitation is hindered kinetically, which also becomes difficult with increasing temperature. It is interesting to investigate whether truly equilibrium nanoalloys can exist in multicomponent alloys with HEGBs, which is suggested by Fig. 1a, but not yet verified experimentally.

Furthermore, a first-order premelting transition can result in a discontinuous increase in the GB excess entropy to accelerate the GB energy reduction with increasing temperature (Fig. 1a, albeit that studies showed GB structural disordering can often increase GB mobilities⁴⁴). Likewise, a first-order adsorption transitions can also cause a discontinuous increase in the GB adsorption (*a.k.a.* segregation), which accelerates the GB energy reduction with increasing chemical potential (Fig. 2b)^{23, 29, 47}. It will be exciting to seek coupled GB disordering or adsorption transitions in HEGBs to further accelerate the γ_{GB} reduction (i.e., increase the effective GB entropy) to potentially achieve zero GB energy within the solid solubility limit (to realize nanoalloys with equilibrium grain sizes at a true thermodynamic equilibrium).

We should develop quantitative models for the combined thermodynamic and kinetic stabilization of nanoalloys at high temperatures via utilizing HEGBs, following the concept shown in Fig. 3. We should also further explore the unique characters of HEGBs beyond thermodynamic and kinetic properties.

A further extension is to investigate other types of high-entropy interfaces beyond GBs. For example, can we use high-entropy surfaces to stabilize nanoparticles for high-temperature catalysis or other applications?⁵² Do high-entropy surfaces (or solid-solid heterointerfaces) have unique properties?

Received: 29 August 2022; Accepted: 20 January 2023;

Published online: 03 February 2023

References

1. Yeh, J. W. et al. Nanostructured high-entropy alloys with multiple principal elements: Novel alloy design concepts and outcomes. *Adv. Eng. Mater.* **6**, 299–303 (2004).
2. Cantor, B., Chang, I., Knight, P. & Vincent, A. Microstructural development in equiatomic multicomponent alloys. *Mater. Sci. Eng. A* **375**, 213–218 (2004).
3. Miracle, D. B. & Senkov, O. N. A critical review of high entropy alloys and related concepts. *Acta Materialia* **122**, 448–511 (2017). **A critical review paper discussed the key concepts in high-entropy alloys (HEAs).**
4. Wright, A. J. & Luo, J. A step forward from high-entropy ceramics to compositionally complex ceramics: A new perspective. *J. Mater. Sci.* **55**, 9812–9827 (2020). **A critical review and perspective paper discussed the key**

- concepts in high-entropy ceramics (HECs) and compositionally complex ceramics (CCCs).**
- Gild, J. et al. High-entropy metal diborides: A new class of high-entropy materials and a new type of ultrahigh temperature ceramics. *Sci. Rep.* **6**, 37946 (2016).
 - Qin, M. et al. 21-component compositionally complex ceramics: Discovery of ultrahigh-entropy weberite and fergusonite phases and a pyrochlore-weberite transition. *J. Adv. Cer.* **11**, 641–655 (2022).
 - Rost, C. M. et al. Entropy-stabilized oxides. *Nat. Commun.* **6**, 8485 (2015).
 - Zhou, N., Hu, T. & Luo, J. Grain boundary complexions in multicomponent alloys: Challenges and opportunities. *Curr. Opin. Solid State Mater. Sci.* **20**, 268–277 (2016). **A perspective paper discussed grain boundary complexions (a.k.a. 2D interfacial phases) and GB transitions in multicomponent alloys and first proposed the concept of high-entropy grain boundaries (HEGBs) with one numerical example as a future perspective.**
 - Zhou, N., Hu, T., Huang, J. & Luo, J. Stabilization of nanocrystalline alloys at high temperatures via utilizing high-entropy grain boundary complexions. *Scripta Materialia* **124**, 160–163 (2016). **The first research paper proposed high-entropy grain boundaries (HEGBs) and demonstrated the use of HEGBs to stabilize nanocrystalline alloys at high temperatures.**
 - Praveen, S. & Kim, H. S. High-entropy alloys: Potential candidates for high-temperature applications—an overview. *Adv. Eng. Mater.* **20**, 1700645 (2018).
 - Lei, Z. et al. Development of advanced materials via entropy engineering. *Scripta Materialia* **165**, 164–169 (2019).
 - Koch, C. C. Nanocrystalline high-entropy alloys. *J. Mater. Res.* **32**, 3435–3444 (2017).
 - Haché, M. J., Cheng, C. & Zou, Y. Nanostructured high-entropy materials. *J. Mater. Res.* **35**, 1051–1075 (2020).
 - Deng, H. et al. A nanocrystalline aluminide medium-entropy alloy with high thermal stability via entropy and boundary engineering. *Mater. Sci. Eng.: A* **774**, 138925 (2020).
 - Kaptay, G. Thermodynamic stability of nano-grained alloys against grain coarsening and precipitation of macroscopic phases. *Metallurgical Mater. Transact. A* **50**, 4931–4947 (2019).
 - Gao, P. et al. Ultra-strong and thermally stable nanocrystalline crconi alloy. *J. Mater. Sci. Technol.* **106**, 1–9 (2022).
 - Wang, Z. et al. Thermal stability of the multicomponent nanocrystalline ni-zrnbmta alloy. *J. Alloys Compound.* **862**, 158326 (2021).
 - Zamani, M. R., Mirzadeh, H., Malekan, M., Cao, S. C. & Yeh, J.-W. Grain growth in high-entropy alloys (heas): A review. *High Entropy Alloys Mater.* 1–35, <https://doi.org/10.1007/s44210-022-00002-8> (2022).
 - Liu, T. et al. Stabilizing fe-based nanocrystalline alloys via a high-entropy strategy. *J. Alloys Compounds* **896**, 163138 (2022).
 - Grigorian, C. M. & Rupert, T. J. Multi-principal element grain boundaries: Stabilizing nanocrystalline grains with thick amorphous complexions. *J. Mater. Res.* **37**, 554–566 (2022).
 - Foiles, S. M. Temperature dependence of grain boundary free energy and elastic constants. *Scripta Materialia* **62**, 231–234 (2010).
 - Cantwell, P. R. et al. Overview no. 152: Grain boundary complexions. *Acta Materialia* **62**, 1–48 (2014).
 - Zhou, N., Yu, Z., Zhang, Y., Harmer, M. P. & Luo, J. Calculation and validation of a grain boundary complexion diagram for Bi-doped Ni. *Scripta Materialia* **130**, 165–169 (2017).
 - Wynblatt, P. & Chatain, D. Anisotropy of segregation at grain boundaries and surfaces. *Metallurgical Mater. Transact. a-Phys. Metallurgy Mater. Sci.* **37A**, 2595–2620 (2006).
 - Lejček, P., Všianská, M. & Šob, M. Recent trends and open questions in grain boundary segregation. *J. Mater. Res.* **33**, 2647–2660 (2018).
 - Černý, M., Šesták, P., Všianská, M. & Lejček, P. On agreement of experimental data and calculated results in grain boundary segregation. *Metals* **12**, 1389 (2022).
 - Lejček, P., Hofmann, S., Všianská, M. & Šob, M. Entropy matters in grain boundary segregation. *Acta Materialia* **206**, 116597 (2021).
 - Seah, M. P. Grain boundary segregation. *J. Phys. F: Metal Phys.* **10**, 1043–1064 (1980).
 - Luo, J., Cheng, H., Asl, K. M., Kiely, C. J. & Harmer, M. P. The role of a bilayer interfacial phase on liquid metal embrittlement. *Science* **333**, 1730–1733 (2011).
 - Luo, J., Gupta, V. K., Yoon, D. H. & Meyer, H. M. Segregation-induced grain boundary premelting in nickel-doped tungsten. *Appl. Phys. Lett.* **87**, 231902 (2005).
 - Koch, C. C., Scattergood, R. O., Darling, K. A. & Semones, J. E. Stabilization of nanocrystalline grain sizes by solute additions. *J. Mater. Sci.* **43**, 7264–7272 (2008).
 - Kalidindi, A. R., Chookajorn, T. & Schuh, C. A. Nanocrystalline materials at equilibrium: a thermodynamic review. *JOM* **67**, 2834–2843 (2015).
 - Cahn, J. W. The impurity drag effect in grain boundary motion. *Acta Metallurgica et Materialia* **10**, 789–798 (1962).
 - Lücke, K. & Stüwe, H. P. In *Recovery and recrystallization of metals (interscience publishers, new york)* (ed. Himmel, L.) 171–210 (1963).
 - Wei, S., He, F. & Tasan, C. C. Metastability in high-entropy alloys: a review. *J. Mater. Res.* **33**, 2924–2937 (2018).
 - Xing, W., Kalidindi, A. R. & Schuh, C. A. Preferred nanocrystalline configurations in ternary and multicomponent alloys. *Scripta Materialia* **127**, 136–140 (2017).
 - Li, L. et al. Segregation-driven grain boundary spinodal decomposition as a pathway for phase nucleation in a high-entropy alloy. *Acta Materialia* **178**, 1–9 (2019).
 - Luo, J. Stabilization of nanoscale quasi-liquid interfacial films in inorganic materials: a review and critical assessment. *Critic. Rev. Solid State Mater. Sci.* **32**, 67–109 (2007).
 - Schuler, J. D., Donaldson, O. K. & Rupert, T. J. Amorphous complexions enable a new region of high temperature stability in nanocrystalline ni-w. *Scripta Materialia* **154**, 49–53 (2018).
 - Grigorian, C. M. & Rupert, T. J. Thick amorphous complexion formation and extreme thermal stability in ternary nanocrystalline cu-zr-hf alloys. *Acta Materialia* **179**, 172–182 (2019).
 - Khalajhedayat, A., Pan, Z. & Rupert, T. J. Manipulating the interfacial structure of nanomaterials to achieve a unique combination of strength and ductility. *Nat. Commun.* **7**, 10802 (2016).
 - Wu, G., Chan, K.-C., Zhu, L., Sun, L. & Lu, J. Dual-phase nanostructuring as a route to high-strength magnesium alloys. *Nature* **545**, 80–83 (2017).
 - Shi, X. & Luo, J. Grain boundary wetting and prewetting in ni-doped mo. *Appl. Phys. Lett.* **94**, 251908 (2009).
 - Dillon, S. J., Tang, M., Carter, W. C. & Harmer, M. P. Complexion: A new concept for kinetic engineering in materials science. *Acta Materialia* **55**, 6208–6218 (2007).
 - Hu, T., Yang, S., Zhou, N., Zhang, Y. & Luo, J. Role of disordered bipolar complexions on the sulfur embrittlement of nickel general grain boundaries. *Nat. Commun.* **9**, 2764 (2018).
 - Luo, Z. et al. A highly asymmetric interfacial superstructure in wc: Expanding the classic grain boundary segregation and new complexion theories. *Mater. Horizons* **7**, 173–180 (2020).
 - Yu, Z. et al. Segregation-induced ordered superstructures at general grain boundaries in a nickel-bismuth alloy. *Science* **358**, 97–101 (2017).
 - Hu, C. & Luo, J. Data-driven prediction of grain boundary segregation and disordering in high-entropy alloys in a 5D space. *Mater. Horizons* **9**, 1023–1035 (2022).
 - Luo, J. Computing grain boundary “phase” diagrams. *Interdisciplinary Materials* **2**, 137–160, <https://doi.org/10.1002/idm2.12067> (2023). **A perspective paper reviewed a series of transformative studies to compute grain boundary “phase” diagrams (including predicting the properties of grain boundaries in high-entropy alloys) and related concepts of grain boundary disordering and transitions, with a discussion on extending this research to high-entropy grain boundaries (HEGBs) in the outlook section.**
 - Weissmüller, J. Alloy effects in nanostructures. *Nanostructured Mater.* **3**, 261–272 (1993).
 - Kirchheim, R. Grain coarsening inhibited by solute segregation. *Acta Materialia* **50**, 413–419 (2002).
 - Yao, Y. et al. High-entropy nanoparticles: Synthesis-structure-property relationships and data-driven discovery. *Science* **376**, eabn3103 (2022).

Acknowledgements

We gratefully acknowledge the support by the U.S. Army Research Office (Grant No. W911NF2210071, managed by Dr. Michael P. Bakas, in the Synthesis & Processing program).

Author contributions

J.L. conceived the initial concepts and basic theory of HEGBs and wrote the paper. N.Z. assisted the detailed analysis to test the concepts and theory in his Ph.D. thesis research with J.L..

Competing interests

The authors declare no competing interests.

Additional information

Correspondence and requests for materials should be addressed to Jian Luo.

Peer review information *Communications Materials* thanks the anonymous reviewers for their contribution to the peer review of this work. Primary Handling Editor: John Plummer.

Reprints and permission information is available at <http://www.nature.com/reprints>

Publisher's note Springer Nature remains neutral with regard to jurisdictional claims in published maps and institutional affiliations.



Open Access This article is licensed under a Creative Commons Attribution 4.0 International License, which permits use, sharing, adaptation, distribution and reproduction in any medium or format, as long as you give appropriate credit to the original author(s) and the source, provide a link to the Creative Commons license, and indicate if changes were made. The images or other third party material in this article are included in the article's Creative Commons license, unless indicated otherwise in a credit line to the material. If material is not included in the article's Creative Commons license and your intended use is not permitted by statutory regulation or exceeds the permitted use, you will need to obtain permission directly from the copyright holder. To view a copy of this license, visit <http://creativecommons.org/licenses/by/4.0/>.

© The Author(s) 2023